Journal of Engineering Physics and Thermophysics, Vol. 74, No. 4, 2001

NUMERICAL PREDICTION OF THE FLOW FIELD NEAR THE TIP OF A ROTATING TURBINE BLADE

S. Han, B. Han, P. Jin, and R. J. Goldstein UDC 532.517.2

Numerical analysis of the three-dimensional flow fields in an annual cascade with tip clearance and rotation and in a linear cascade is carried out. A comparison with flow visualization verifies the computational result. The comparison indicates that the numerical analysis captures the separation on the tip edge of the pressure side of the blade and the flow direction over the tip surface. However, it does not properly indicate the separation on the leading edge of the suction side. Rotation weakens the leakage flow so that the size of the separation bubble decreases on the tip surface. Large tip clearance increases leakage flow so that the tip vortex is larger and moves to the suction side.

Introduction. To increase the efficiency and power of modern gas turbine, it is necessary to understand the flow and heat transfer in the turbine. For example, the flow field and separation on a blade tip affect the heat transfer on the blade tip surface. Experimental studies on flow patterns through turbine passages are reviewed by Sieverding [1] and Langston [2]. There is general agreement on the flow patterns, but disagreement on the number of the vortices in the passage. Jabbari et al. [3] and H. P. Wang [4] (Fig. 1) tried to clarify the flow patterns by comparing results of flow visualization and mass transfer measurements. Their results showed the initiation and evolution of horseshoe and passage vortices in the passage. Even though those studies improve the understanding of the flow patterns in the turbine passage, most of them are performed in a linear cascade without tip clearance.

The influence of the tip gap on flow and heat transfer was studied by Metzger et al. [5] and Moore et al. [6]. These studies focus on the flow pattern in the gap, but the interaction between the leakage flow and the flow in the passage is not fully studied. Several three-dimensional numerical analyses [7–9] on the flow in the turbine passage have been performed. Liu and Bozzola [7] calculate the three-dimensional flow field in a passage with tip clearance and rotation, but the computational domain is for a linear cascade. The computation by Basson, et al. [8] is carried out in an annular passage with tip clearance, but rotation is not considered.

In the present study, the three-dimensional flow field in an annular turbine rotor passage is numerically studied. Effects of rotation are indicated by comparing the calculation results with a linear cascade. Calculations with four different tip clearances – 1%, 2%, 4%, and 7% of blade chord – are performed to find out the effects of tip clearance though realistically only the smallest value might occur in an operating turbine. The results are verified by comparison with a flow visualization experiment.

Numerical Analysis. *Numerical code*. A three-dimensional commercial CFD code, TASCflow developed by AEA technology, is used for this study. This code solves the Reynolds-averaged Navier–Stokes equations in stationary and rotating coordinates. It is based on a boundary-fitted, nonorthogonal and curvilinear structured grid system. This particular code was chosen with recommendation of industrial consultant. It

Heat Transfer Laboratory, Department of Mechanical Engineering, University of Minnesota, Minneapolis, USA; email: bshan@me.umn.edu. The article submitted June, 29, 2000. Translated from Inzhenerno-Fizicheskii Zhurnal, Vol. 74, No. 4, pp. 14–22, July–August, 2001. Original article submitted September 29, 2000.

1062-0125/01/7404-0859$25.00

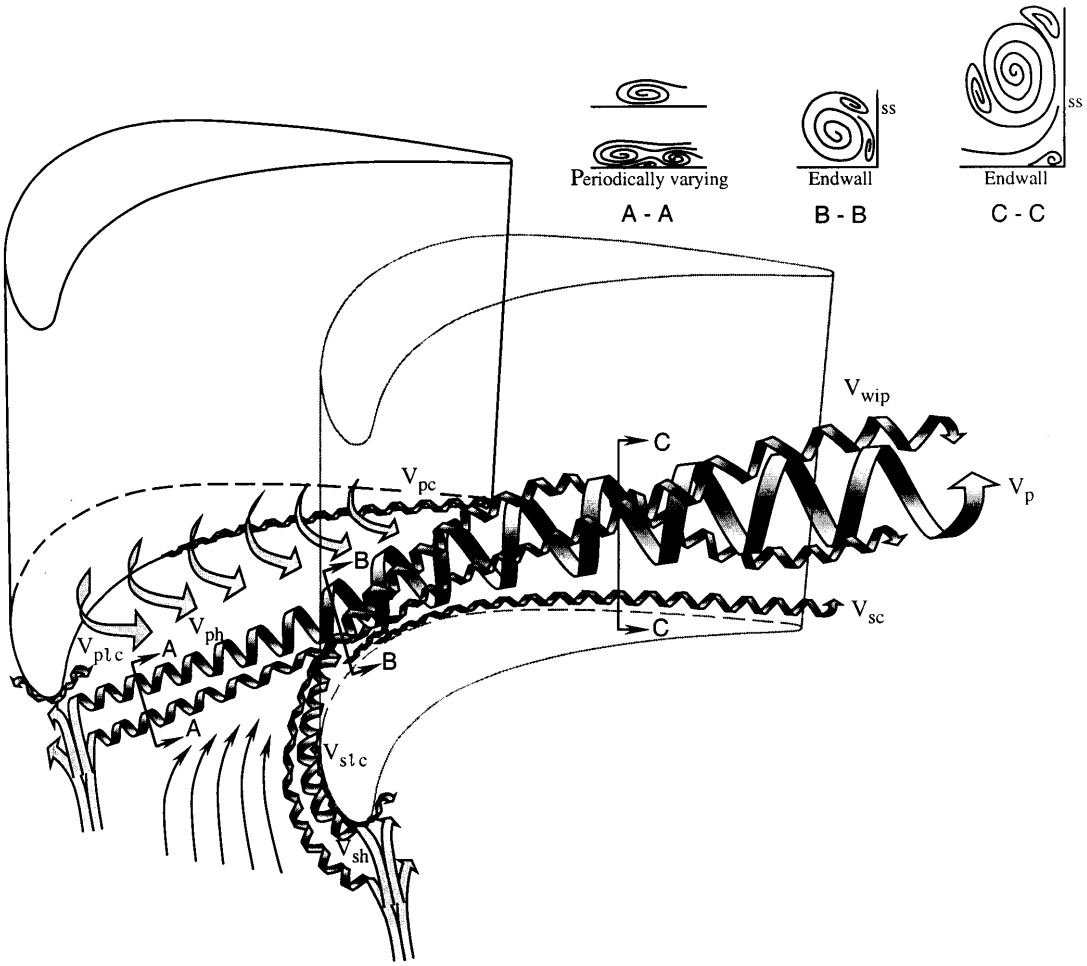

Fig. 1. Flow structure in turbine cascade from H. P. Wang et al. (1997): V_{sh}, suction side leg of horseshoe vortex system; V_{ph}, pressure side leg of horseshoe vortex system; V_p, passage vortex; V_{wip}, wall vortex induced by the passage vortex; V_{slc}, suction side leading edge corner vortex; V_{plc}, pressure side leading edge corner vortex; V_{sc}, suction side corner vortex; V_{pc}, pressure side corner vortex.

TABLE 1. Detailed Geometry of Calculation Domain

Annular cascade	
Hub radius	0.335 m
Blade span	0.123 m
Axial blade chord, C_a	0.129 m
Number of blades	29
Tip clearance, τ/C_a	1%, 2%, 4%, and 7%
Linear cascade	
Hub radius	0.195 m
Blade span	0.138 m
Axial blade chord, C_{lin}	0.130 m
Tip clearance, τ/C_{lin}	0.86%, 1.72%, 3.45%, and 6.9%

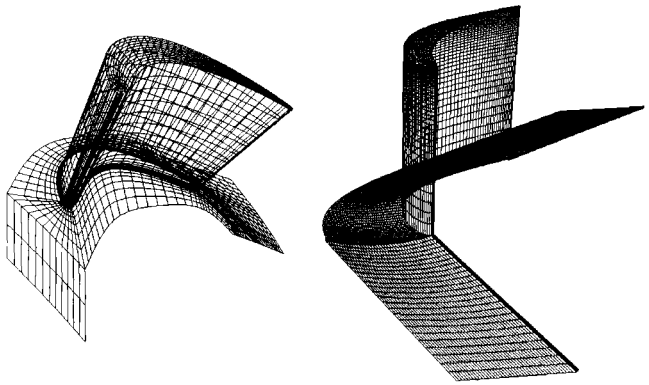

Fig. 2. Computational grids for annular central one blade and linear cascade in hollow section between two blades.

TABLE 2. Boundary Condition and Computational Parameter

Annular cascade	
Rotating speed	1000 rpm
Relative inlet velocity	42.4 m/sec
Inlet flow angle	43.17^{o}
Turbulence intensity	1.0%
Length scale	0.005 m
Linear cascade	
Inlet velocity	20 m/sec
Inlet flow angle	35^{o}
Turbulence intensity	1.0%
Length scale	0.005 m

is widely used in the gas turbine industry which would permit our result to be incorporated in design calculation.

Computation Grid, Boundary and Inlet Conditions. The geometry of the annual blade modeled in this study is based on the Axial Flow Turbine Research Facility at the Turbomachinery Laboratory of Pennsylvania State University. The commercial grid generator, Turbogrid from AEA technology, is used to construct the computational grid. The multi-grid structure is generated to control the grid distribution in the interesting part of blade. An O-grid to make a dense grid near the surface is used around the blade and a C-grid is used in the blade passage and around the leading edge of the blade. Two H-grid blocks are used at the trailing edge. Four different tip clearances are used for this study. The geometry of the linear blade is based on the blade in a linear cascade in the Heat transfer Laboratory of the University of Minnesota. The computational grid is generated by CFX-build 4 that is developed by AEA Technology. The grid system is in the central passage configuration. The blade geometry is listed in Table 1. The computational grids are presented in Fig. 2.

For the annular blade. At the inlet of the domain, a uniform velocity boundary condition is assumed. Periodic boundary conditions are assigned on the pitchwise direction. The inlet Reynolds number based on the relative inlet velocity and chord length is 3.8×10^5. The standard k–ε model is employed for the turbulence model.

For the linear blade. At the inlet of the linear cascade, a uniform velocity is assumed. The exit Reynolds number based on the exit velocity and blade chord is 6.4×10^5. The detailed conditions are listed in Table 2.

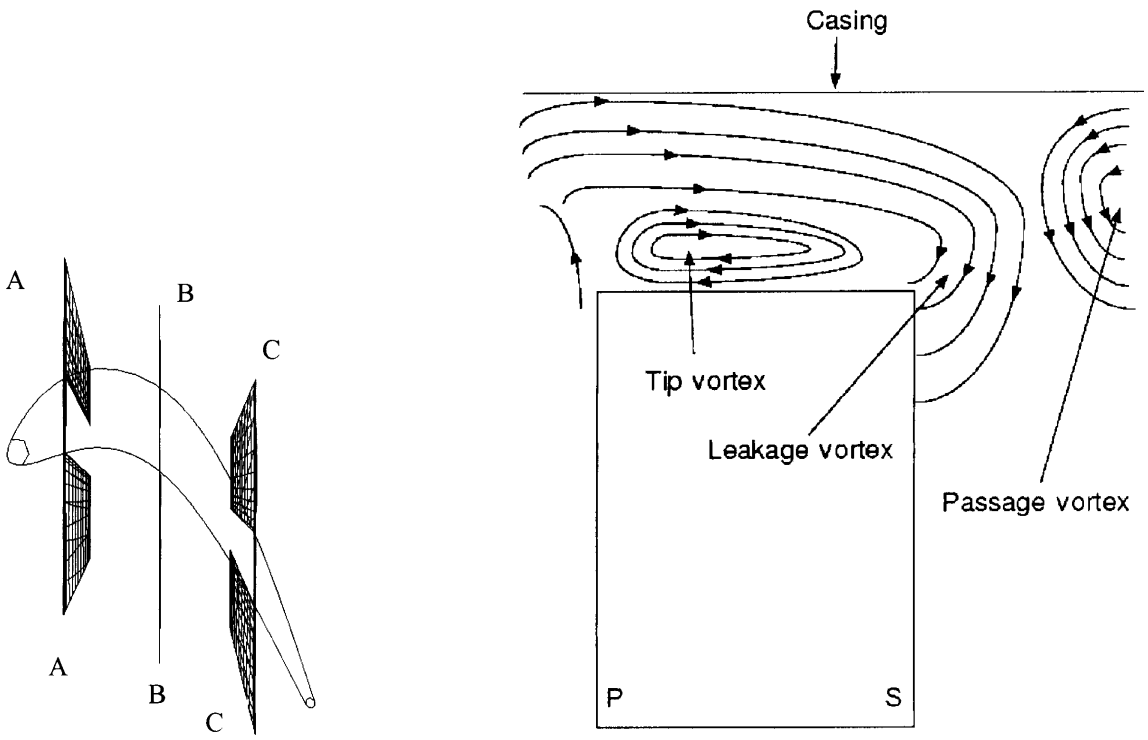

Fig. 3. Location of cross sections.

Fig. 4. The schematic shape of vortices.

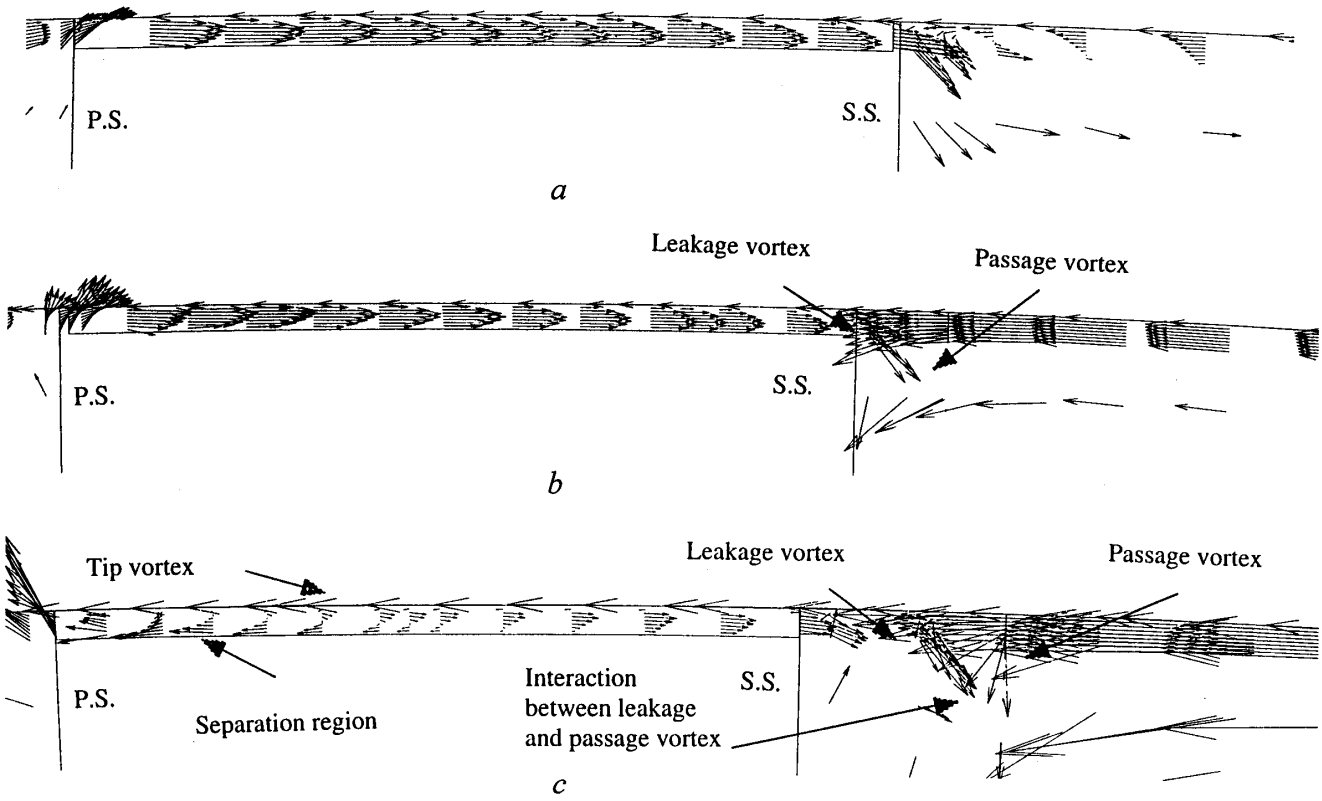

Fig. 5. Velocity vector in tip clearance (1%) with rotation: a) A–A section; b) B–B section; c) C–C section.

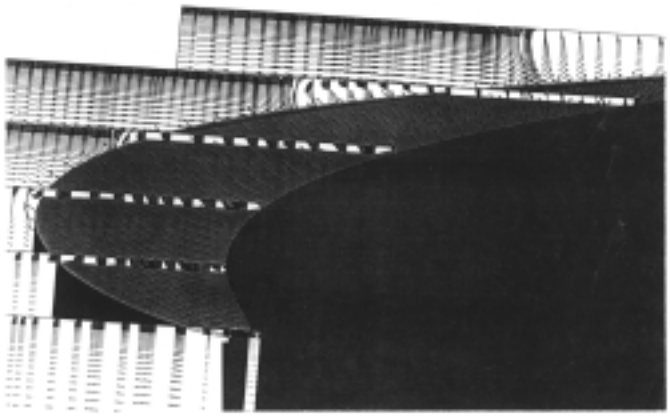

Fig. 6. Velocity vector in tip clearance (0.86%) without rotation.

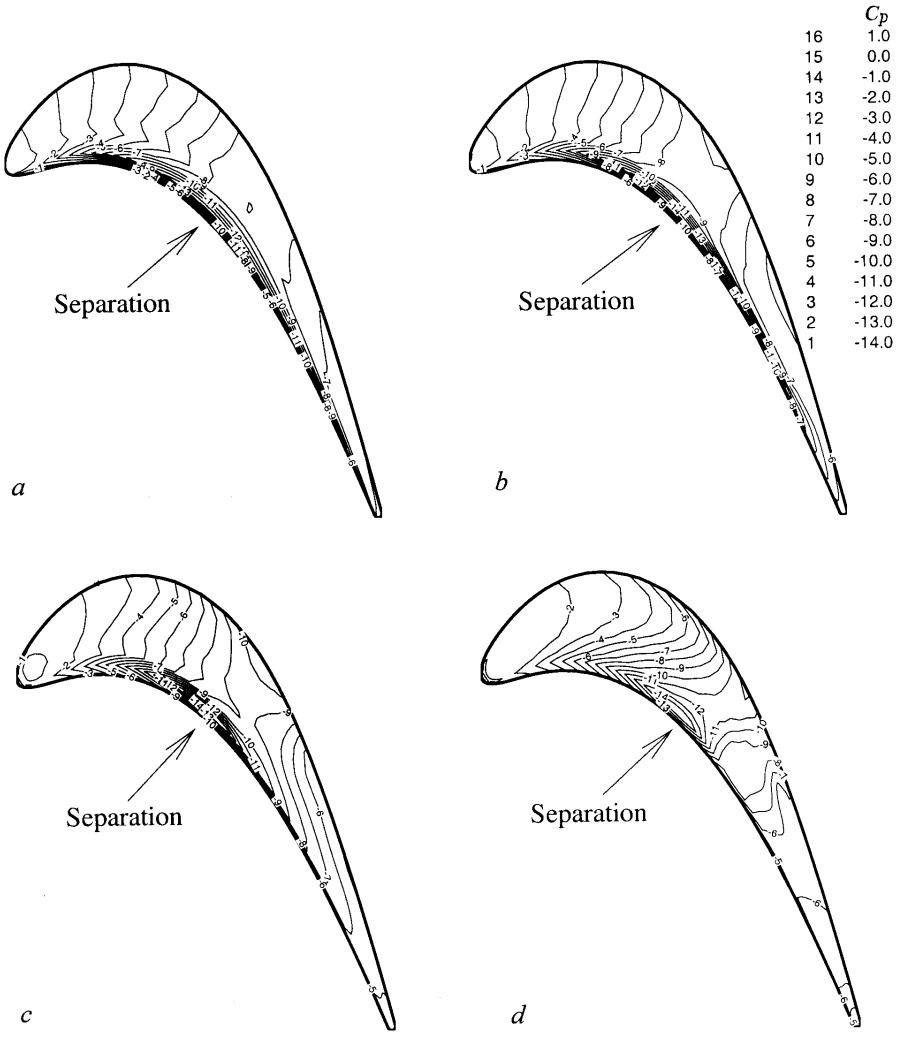

Fig. 7. Static pressure distributions on tip without rotation: τ/C_{lin} = 0.86%; b) 1.72; c) 3.45; d) 6.9.

Results and Discussion. Results are for the annular blade with rotation for tip clearances of 1%, 2%, 4%, and 7%, and for the linear blade without rotation for tip clearances of 0.86%, 1.72%, 3.45%, and 6.9%. Three cross sectional planes, each are parallel to the inlet, are used to visualize the relative flow vector for

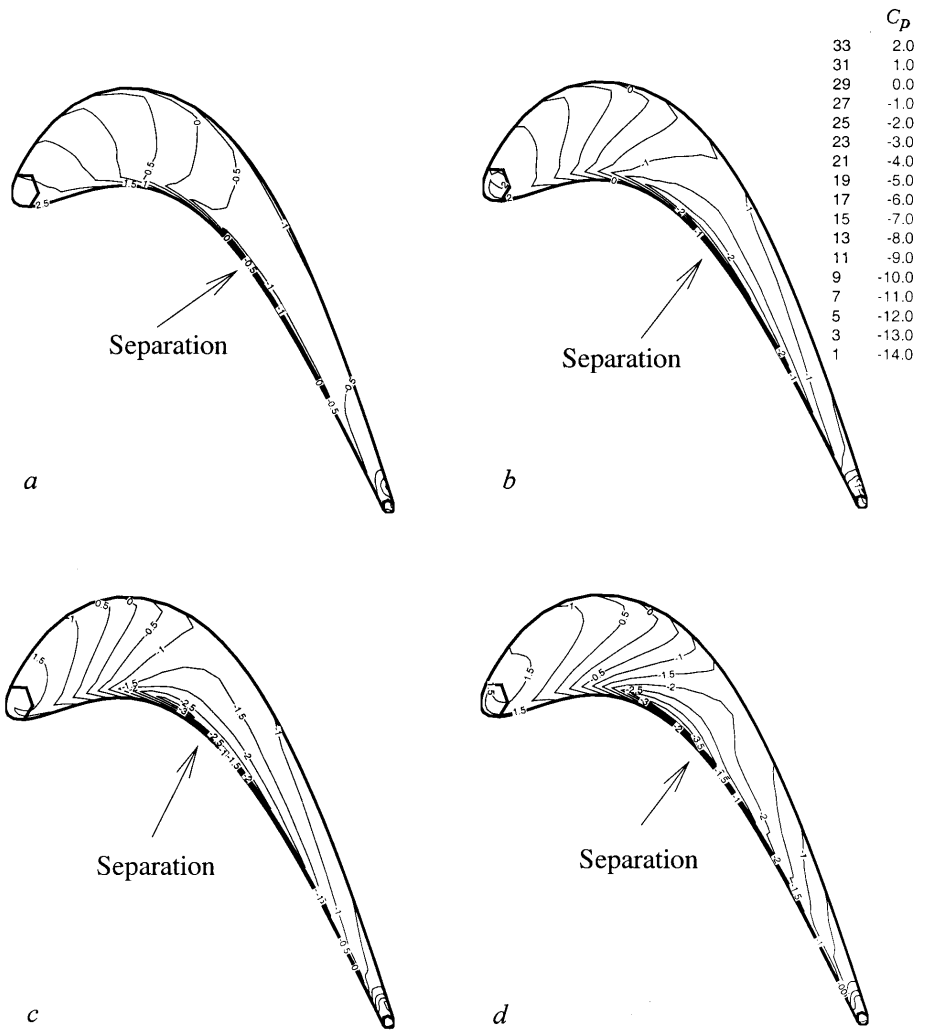

Fig. 8. Static pressure distributions on tip with rotation: a) τ/C_a = 1%; b) 2; c) 4; d) 7.

the rotating annular blade at the different tip clearances. The locations of the planes are 20% (A–A), 50% (B–B), and 80% (C–C) of the axial chord (Fig. 3). Relative velocity vectors near the tip are presented at the different tip clearances for the linear blade without rotation. Figure 4 is a representation of the tip vortex, leakage vortex, and passage vortex as they occur in some of the sections.

Effect of rotation. The velocity distributions for 1% tip clearance with rotation are presented in Fig. 5. Leakage flow comes from the pressure side and goes out to the suction side at A–A and B–B. At B–B and C–C, a separation bubble is observed near pressure side on tip. In Fig. 6, the velocity vectors are presented at similar cross sections for 0.86% tip clearance without rotation.

Even though two results come from different conditions and geometries, very similar trends are observed. The velocity distributions in the different cross sections show good agreement to the results with rotation. A thin shear layer is observed within the tip clearance due to the relative motion of the casing with respect to the blade. The velocity difference near the casing results from the rotation. The location where the passage vortex meets the leakage vortex in section C–C is closer to the suction side when rotation is present. Thus the rotation moves the passage vortex closer to the leakage vortex, and intensifies the interaction between the vortices.

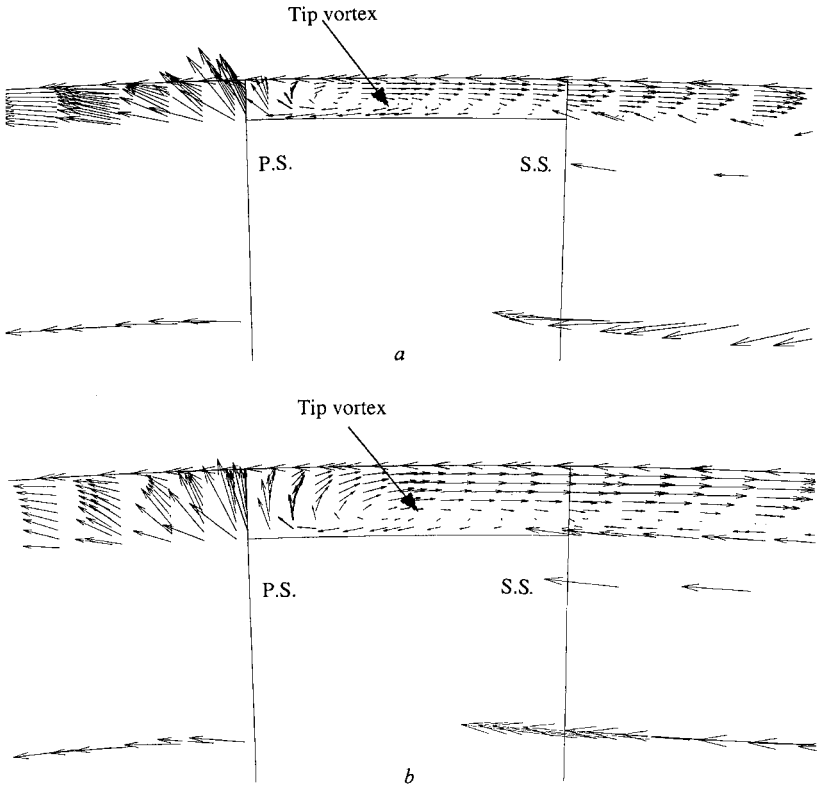

Fig. 9. Velocity vector with rotation for C–C section in tip clearance: a) 2%; b) 4.

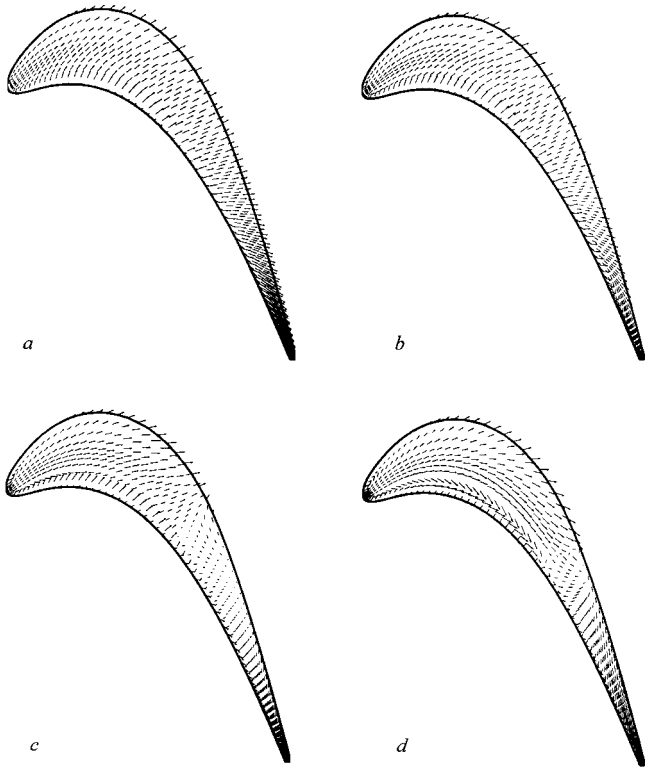

Fig. 10. Velocity vector distributions on the tip surface without rotation: a) τ/C_{lin} = 0.86%; b) 1.72; c) 3.45; d) 6.9.

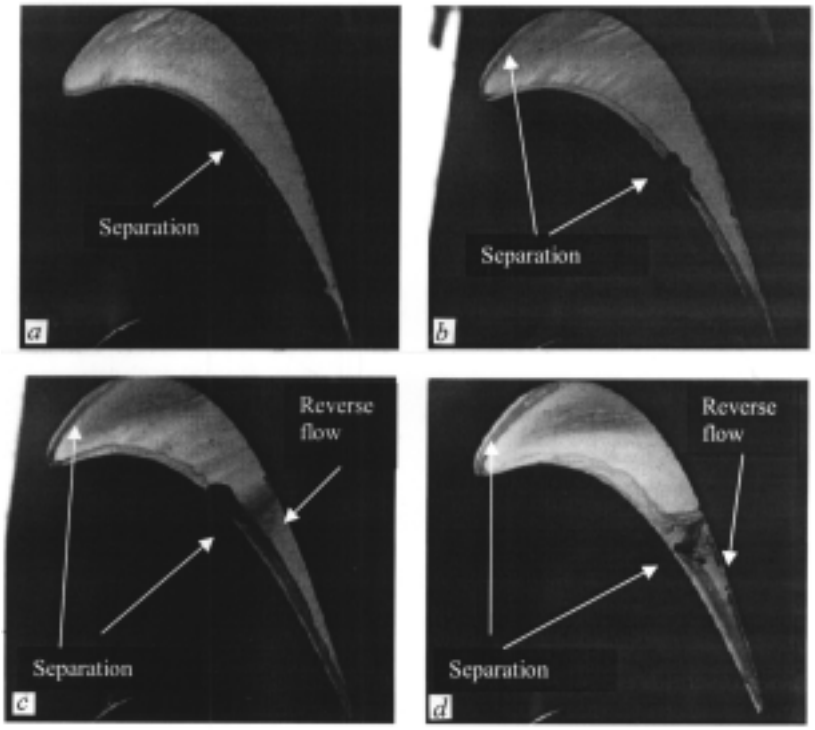

Fig. 11. Flow visualization on tip with different tip clearance: a) τ/C_{lin} = 0.86%; b) 1.72; c) 3.45; d) 6.9.

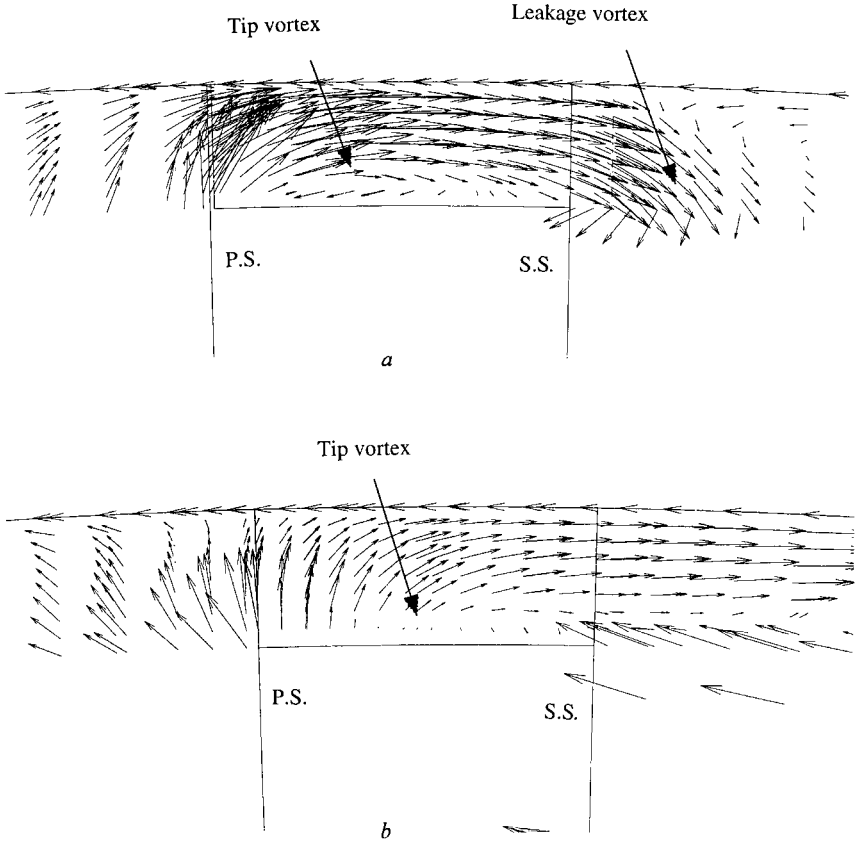

Fig. 12. Velocity vector in tip clearance (7%) with rotation: a) B–B section; b) C–C section.

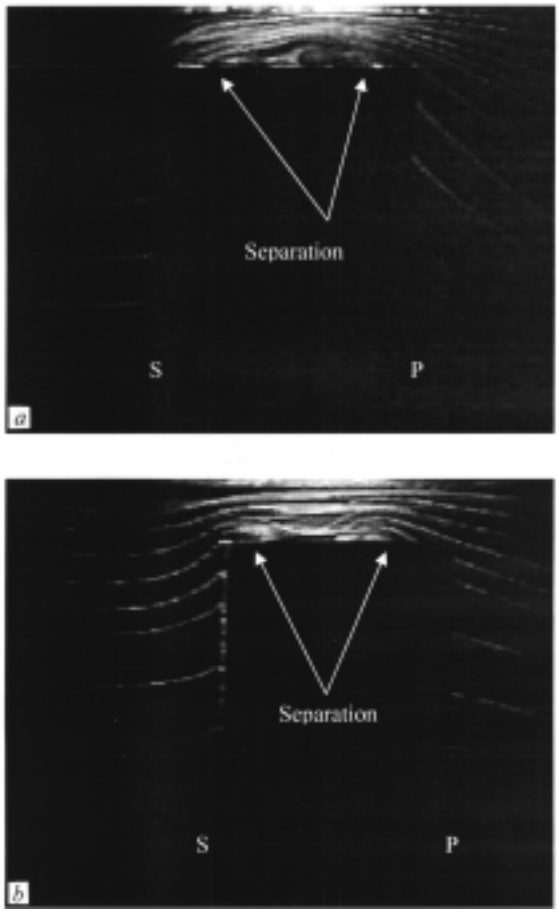

Fig. 13. Flow visualization in tip clearance (6.9%): a) B–B section; b) C–C section.

The static pressure differences with and without rotation observed in the tip clearance (0.86% and 1%) are shown in the nondimensional values (C_P) to make comparison easy. The pressure distribution with rotation indicates two low-pressure regions on both the pressure and the suction sides near B–B. The lowest pressure is observed near the pressure side without rotation. The difference of static pressure is from the momentum loss due to rotation. The momentum of the flow is used to rotate blades so that the leakage flow with rotation is weaker than that without rotation. It affects the differences in the static pressure on the tip surface. This is also true for the other tip clearances.

Effect of tip clearance. Static pressure plots on the tip with rotation are presented for the different tip clearances in Fig. 8. Low-pressures are observed near the pressure side for all tip clearances. This grows from the pressure to the suction side near B–B and decreases as the tip clearance gets larger. A high pressure is observed near leading edge. Because there is the stagnation point near the leading edge, the magnitude and location of high pressure are independent of tip clearance. The lowest pressure is observed with the largest tip clearance (7%). Because the large tip clearance increases leakage flow, it increases vortex intensity and finally induces lower pressure on the tip. The lower pressure region agrees well with the separation bubble observed in flow visualization.

The shape of tip vortex in Fig. 9 shows good agreement with the separation region in Fig. 6. As tip clearance gets larger, tip vortex gets larger and the center of the vortex moves to suction side. The growth of low-pressure region in Fig. 6 agrees with the growth and movement of tip vortex in Fig. 9. It is due to the increase of leakage flow for increased tip clearance.

Comparison with flow visualization. Comparison is made between computations in Figs. 7 and 10, and flow visualization in Fig. 11, all for the linear cascade without rotation. In the flow visualization, as the tip clearance increases from 0.86% to 1.72%, the separation bubbles increase on the tip edge of pressure. The increase of the separation bubbles is well predicted by computation in Fig. 7. The low-pressure zone near the mid-chord on the tip edge of the pressure side, also appears in computation with tip clearance of 3.45%. The reverse flows and accumulation of oil on the second half of the tip surface are well predicted in computation in Fig. 8. Also the separation along the pressure side edge is well predicted, however, the separation of the tip edge of suction side near leading edge is not well captured by the computation.

It can also be seen that for the two small tip clearances, the leakage flow mostly comes from the pressure side and passes though the clearance gap with little change in flow direction. While for two large clearances, the turning of leakage flow on the first half part of tip is clearly shown, and the reverse flow from suction side on the second half tip is shown. This also agrees with flow visualization. For the two largest tip clearances, visualization shows the oil accumulations on the mid-tip and a different direction pattern of oil on the second half of tip.

Figure 13 shows the flow visualization with 6.9% tip clearance near B–B and C–C section of calculation. The visualization shows two tip vortexes on the tip surface, but computation results show only one tip vortex near the pressure side edge of tip clearance (Fig. 12).

Conclusions. The flow field in the tip clearance and the pressure distributions are studied using a commercial code. The computations are performed to investigate the effect of rotation and tip clearance. The analysis is verified by comparison with flow visualization.

1. On the tip, the static pressure without rotation is smaller than that with rotation for the same tip clearance. The leakage flow without rotation is faster and stronger than that with rotation. With rotation, the main flow uses the momentum to move the blades so that the leakage flow is weaker than that without rotation.

2. For small tip clearance, the leakage flow comes in from pressure side and goes out to the suction side. At larger tip clearance, some leakage flow enters from the suction side and exits along the chord direction. This flow has strong interaction with leakage flow from the pressure side and makes the tip vortex. The computation shows only one tip vortex on the tip surface. It does not catch other tip vortexes.

3. The comparison between the static pressure distribution and flow visualization indicates a lower pressure region occurring in the separation region. This is located on the pressure side edge of the tip surface. As tip clearance increases, this region gets wider and there is a smaller pressure distribution in the mid-tip. The computation does not indicate the separation which were observed on the leading edge of suction side.

Acknowledgments. The present study is supported by U.S Department of Energy through the Advanced Gas Turbine System Research (AGTSR) program. The authors would like to thank to AEA Technology for providing TASCflow and Dr. C. Camci for providing information about the blade geometry for the rotating blade. All computations were carried out in the Scientific Development and Visualization Laboratory (SDVL) at the University of Minessota Supercomputing Institute.

NOTATION

C_{lin}, axial chord length of linear blade; C_a, axial chord length of annular blade; Re_{ex}, exit Reynolds number based on chord and exit velocity; τ, tip clearance (distance from blade tip to casing); $C_P = \dfrac{P - P_\infty}{0.5\,\rho U_\infty^2}$, friction coefficient.

REFERENCES

1. C. Sieverding, *J. Eng. Gas Turbines Power*, **107**, 248–257 (1985).
2. L. Langston, *AGARD*, No. 496 (1990).
3. M. Jabbari, R. Goldstein, K. Marston, and E. Eckert, *Wärme- und Stoffübertragung*, **27**, 51–59 (1991).
4. H. P. Wang, S. J. Olson, R. J. Goldstein, and E. R. Eckert, *Trans. ASME, J. Turbomachinery*, **119**, 1–8 (1997).
5. D. Metzger, M. Dunn, and C. Hah, *J. Turbomachinery*, **113**, 502–507 (1991).
6. J. Moore, J. G. Moore, H. Henry, and U. Chaudhry, *J. Turbomachinery*, **111**, 301–309 (1989).
7. J. Liu and R. Bozzola, *AIAA J.*, **31**, 2068–2074 (1993).
8. A. H. Basson, R. F. Kunz, and B. Lakshminarayana, *J. Propulsion Power*, **9**, 59–66 (1993).
9. B. Han and R. J. Goldstein, in: *Proc. Symp. on Energy Engineering in the 21st Century*, Vol. 1 (2000), pp. 206–211.